Multiwavelength Optically Controlled Phased-Array Antennas

Dennis T. K. Tong and Ming C. Wu, *Member, IEEE*

***Abstract*— A novel multiwavelength scheme is proposed and demonstrated for one-dimensional (1-D) and two-dimensional (2-D) optically controlled phased-array antenna (OCPAA) systems with true time delay (TTD). This hardware-compressive architecture employs a multiwavelength laser source in conjunction with a programmable dispersion matrix (PDM) and switched optical delay lines (SODL's) to generate all the required time delays for beam steering in 2-D phased-array antenna systems. Independent control of elevation and azimuthal scan is achieved by combining wavelength-dependent and wavelength-independent time delays. An experimental prototype of 4 × 2 array with 2-b × 2-b resolution is constructed to demonstrate the feasibility of the multiwavelength OCPPA (MWOCPAA). Broadband linear RF phase shift is measured in both elevation and azimuthal planes over the entire bandwidth of the electro-optic (EO) modulator. System issues such as insertion loss, array size, and channel isolation are discussed. Extension of the multiwavelength scheme to a common transmit/receive (T/R) module with TTD is also described.**

***Index Terms*—Bragg fiber grating, optical beamforming, true time delay, wavelength–division–multiplexed.**

I. Introduction

FIBER OPTICS is very attractive for implementing true time delay (TTD) beamforming networks in phased-array antennas because optical fibers have low attenuation, light weight, high flexibility, broad bandwidth, and immunity to electromagnetic interference (EMI). More importantly, optically controlled phased-array antennas (OCPAA) allow squint-free beam scanning with wide instantaneous bandwidth [1]–[9]. In addition to satisfying the required RF performance, practical OCPAA also needs to be hardware-compressive, robust, manufacturable, and affordable. Recently, there has been a growing interest in applying the wavelength-division multiplexing (WDM) techniques to reduce the complexity of the optical beamforming networks [2]–[9]. Most of WDM schemes employ a tunable laser source in which each wavelength corresponds to a different scan angle [2], [3], [6], [7]. However, the full parallelism of the WDM has not yet been exploited.

Manuscript received December 10, 1996; revised October 9, 1997. This project was supported by DARPA NCIPT, JSEP, and the Parkard Foundation.

The authors are with the Electrical Engineering Department, University of California at Los Angeles (UCLA), Los Angeles, CA 90095-1594 USA (e-mail: wu@ee.ucla.edu).

Publisher Item Identifier S 0018-9480(98)00623-1.

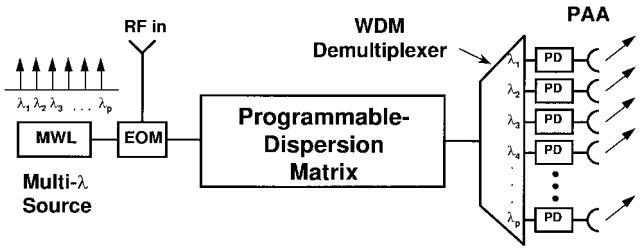

Fig. 1. Schematic diagram of an 1-D MWOCPAA using PDM.

Previously, we have reported a multiwavelength OCPPA (MWOCPAA) which employs a multiwavelength source and a programmable dispersion matrix (PDM) for TTD processing. In contrast to the wavelength-division-multiplexed (WDM) schemes with tunable lasers, the multiwavelength scheme employs a distinctive wavelength to carry the RF signal of each antenna element. The PDM, which is basically a wavelength-dependent tunable optical-delay line, constitutes the common beamforming network for one-dimensional (1-D) MWOCPAA [8], [9]. In this paper, we extend this concept to a two-dimensional (2-D) MWOCPAA system. We begin with a detailed description of the PDM and its application in 1-D MWOCPAA systems. Next, a 2-D MWOCPAA is demonstrated by cascading the PDM with switched optical-delay lines (SODL's). Experimentally, a 4 × 2 MWOCPAA prototype with 2-b × 2-b resolution is demonstrated. The insertion loss in the PDM and its impact on system performance are discussed. The use of optical amplifiers to compensate the PDM insertion loss is investigated. Issues associated with the WDM demultiplexer, such as array size and isolation between elements are also discussed. Finally, we describe the receive mode of MWOCPAA and the possible implementation of a common transmit/receive (T/R) module.

II. MWOCPAA Transmitter in 1-D System

Fig. 1 illustrates the schematic diagram of the 1-D MWOCPAA system with p antenna elements. It comprises: 1) a multiwavelength laser source with p optical wavelengths $\{\lambda_1, \lambda_2, \cdots, \lambda_p\}$; 2) an electro-optic (EO) modulator; 3) a PDM to control the relative time delays τ_{PDM} among different optical wavelengths; and 4) a WDM demultiplexer to route the optical carrier to the corresponding antenna element. The number of optical wavelengths required in this scheme is equal to the number of array elements. Potential candidates for the multiwavelength laser source include monolithically integrated

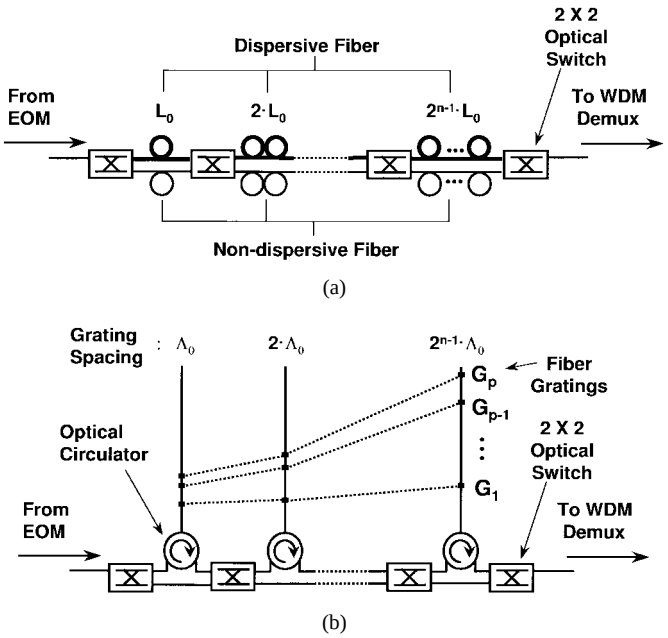

Fig. 2. A n-b PDM implemented with (a) dispersive fiber and (b) Bragg fiber grating.

multiwavelength distributed feedback (DFB) laser arrays [10], [11] and, as will be demonstrated in this paper, monolithic mode-locked semiconductor lasers. The detail of the PDM is shown in Fig. 2. In general, a PDM with n-b resolution requires n dispersive elements, n nondispersive fiber lines, and $(n+1)$ 2×2 optical switches. The optical switches at each PDM stage route the modulated lightwave to either the dispersive element or the nondispersive fiber line. The dispersive element in the PDM can be realized by dispersive fiber [see Fig. 2(a)] or fiber grating [see Fig. 2(b)]. In either case, the relative time delay generated between adjacent optical channels at successive PDM stages increases exponentially, i.e., τ_0, $2\tau_0$, $2^2\tau_0$, $\cdots$, $2^{n-1}\tau_0$. Here, τ_0 is the relative time delay between adjacent optical channels in the first stage of the PDM. If the PDM is implemented with dispersive fiber, the dispersion of the fiber induces a temporal "walk-off" among the optical channels, and τ_0 can be expressed as

$$\tau_0 = D \cdot L_0 \cdot \Delta\lambda \tag{1}$$

where D (ps/km–nm) is the dispersion coefficient of the fiber, L_0 is the length of the fiber in the first stage, and $\Delta\lambda$ is the channel spacing. The length of the dispersive fibers increases exponentially at successive stages, i.e., L_0, $2L_0$, 2^2L_0, $\cdots$, $2^{n-1}L_0$. Equation (1) also indicates that in order to generate a linear relative time delay across the optical channels, a multiwavelength laser source with uniform channel spacing is required. This can be realized by using the mode-locked supermode as the multiwavelength laser source since the wavelength spacing is precisely equal to the mode-locking frequency.

The drawback of dispersive fiber PDM is that long fibers are needed to generate large time delays. Moreover, the time delay is accompanied by dispersion-induced RF signal attenuation and thus the instantaneous bandwidth of the system is limited [12]. This can be solved by employing fiber grating as "tailorable-dispersive" elements in the PDM by fabricating a series of grating reflectors at different positions along the fiber. Each grating G_i reflects a wavelength of the source λ_i, as shown in Fig. 2(b). In this situation, τ_0 is given by

$$\tau_0 = \frac{2 \cdot \Lambda_0 \cdot \eta}{c} \tag{2}$$

where Λ_0 is the grating spacing in the first stage, η is the refractive index of the fiber, and c is the speed of light in free space. Optical circulators are used to route the reflected lightwave to the next stage. The grating spacing at successive stages increases exponentially, i.e., Λ_0, $2\Lambda_0$, $2^2\Lambda_0$, $\cdots$, $2^{n-1}\Lambda_0$. The PDM is highly scalable with scan resolution—the total number of stages in PDM increases logrithmatically with the resolution.

By programming the optical switches, the total relative time delay between adjacent optical channels $\tau_{\rm PDM}$ can be expressed as

$$\tau_{\rm PDM} = \sum_{i=1}^{n} 2^{i-1} \cdot \tau_0 \cdot S_i \tag{3}$$

where $S_i = 0$ or 1 is the state of the ith optical switch. Equation (3) indicates that $\tau_{\rm PDM}$ can vary from zero to $(2^n - 1 \cdot \tau_0)$ in increments of τ_0. The WDM demultiplexer directs λ_i to the ith element of the array, creating a linear time shift of $\{0, \tau_{\rm PDM}, 2\tau_{\rm PDM}, \cdots, (p-1)\cdot\tau_{\rm PDM}\}$ across the array elements. For an array element spacing of d, the beam-steering angle $\theta_{\rm ELEV}$ is

$$\theta_{\rm ELEV} = \sin^{-1}\left(\frac{c \cdot \tau_{\rm PDM}}{d}\right) \tag{4}$$

for all RF frequencies. Equation (4) indicates the squint-free beam-steering operation of TTD systems.

III. MWOCPAA Transmitter in 2-D System

The multiwavelength scheme can be extended to 2-D systems. Here, we demonstrate a 2-D MWOCPAA system by cascading the PDM and the SODL's, similar to those described in [4] and [6]. Fig. 3 shows the schematic diagram of a $p \times q$ 2-D MWOCPAA with n-b $\times$ m-b scanning resolution. The PDM described in the previous section is employed for beam steering in the elevation plane. The WDM signals processed by the PDM are equally split into q columns of the array. Each column consists of an SODL and a WDM demultiplexer. The SODL's control the relative time delays among the columns, and, therefore, beam scanning in the azimuthal plane. The SODL can be cascaded with the PDM because the time delay it introduces is wavelength-independent and will be added to the wavelength-dependent relative time delays among optical wavelengths. Under this configuration, a one-to-one correspondence is established between optical wavelengths and rows of the array, i.e., λ_k is assigned to the kth row of the array.

The principle of SODL is well known [13]. Fig. 4 shows a typical SODL with m-b resolution. Time delays are generated at each stage by the difference in optical path lengths between

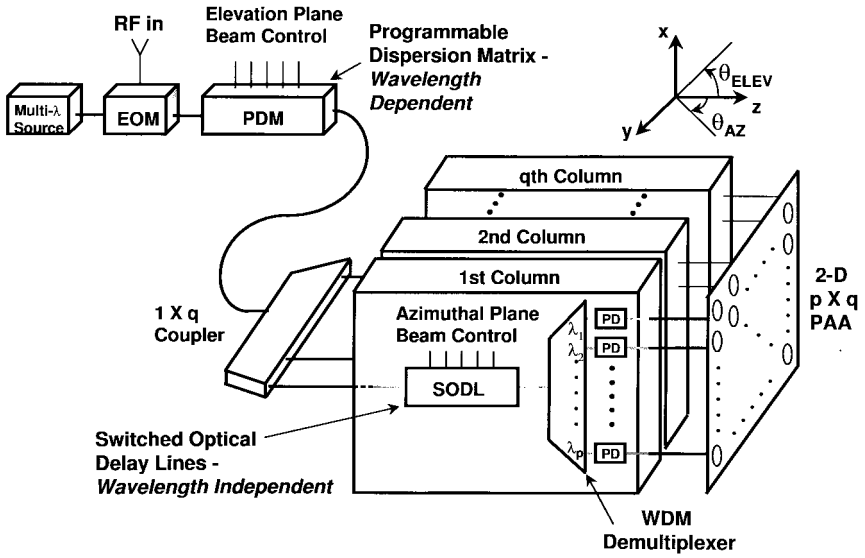

Fig. 3. Schematic diagram of a 2-D $p \times q$ n-b $\times$ m-b MWOCPAA constructed of cascaded PDM and SODL.

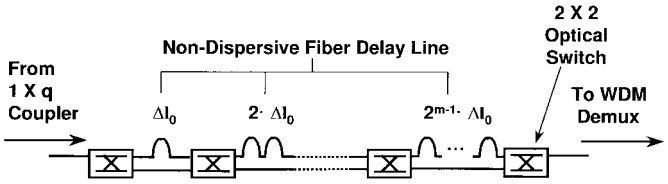

Fig. 4. Schematic diagram of m-b SODL. The difference in length between the upper and lower fiber line at each stage is represented by $\Delta l_0, 2 \cdot \Delta l_0, \cdots, 2^{m-1} \cdot \Delta l_0$.

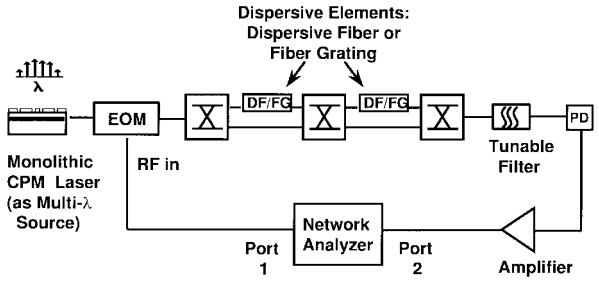

Fig. 5. Experimental setup for RF phase measurement of the 1-D MWOPCAA system. This setup is also used for RF phase measurement in the 2-D MWOCPAA setup.

the upper and the lower fiber delay lines. In particular, the time delay induced at the first stage of the SODL t_0 is

$$t_0 = \frac{\Delta l_0 \cdot \eta}{c} \tag{5}$$

where Δl_0 is the difference in length between the upper and the lower fiber delay lines in the first stage. The SODL can generate a time delay τ_{SODL} from zero to $(2^m - 1 \cdot t_0)$ in an increment of t_0. It is important to note that although the architecture of the dispersive PDM fiber in Fig. 2(a) and the SODL in Fig. 4 are similar, their operating principles are different. In contrast to PDM, the time delays generated by SODL are *wavelength-independent* and a uniform τ_{SODL} is imposed on all the optical wavelengths, while the dispersion in dispersive fiber PDM induces *wavelength-dependent* relative time delays τ_{PDM} among the optical channels. Since all time delays in the azimuthal plane are relative to that of the first column in the array, the SODL attached to the first column can be replaced by a fiber. The length of this fiber should be appropriately matched to compensate for the optical path length of minimum delay in SODL. It should also be mentioned that the SODL associated with each column are different because the time increments in successive SODL's have to increase linearly to preserve the linear time delays across the azimuthal plane during the beam-steering operation.

The steering angle in the elevation plane θ_{ELEV} is related to τ_{PDM} by (4). The steering angle in the azimuthal plane θ_{AZ} is controlled by the time delay between adjacent columns of the array τ_{SODL} as follows:

$$\theta_{\mathrm{AZ}} = \sin^{-1}\left(\frac{c \cdot \tau_{\mathrm{SODL}}}{d}\right). \tag{6}$$

In general, a $p \times q$ 2-D MWOCPAA with n-b $\times$ m-b scanning resolution requires one multiwavelength laser source with p optical wavelength channels, one n-b PDM, one $1 \times q$ optical splitter, $(q-1)$ m-b SODL, and q WDM demultiplexers.

IV. Experiment

To demonstrate the principle of PDM, a 2-b experimental prototype (as shown in Fig. 5) is constructed to measure the relative time delays among the optical channels. In this setup, an 80-GHz monolithic passive colliding-pulse mode-locked (CPM) InGaAs/InGaAsP quantum-well laser is employed as the multiwavelength source [14]. The mode spacing of the CPM laser is 0.60 nm. The reduced mode partition noise in the mode-locked laser makes it a suitable multiwavelength source for our application [15]. To measure the time delays induced by dispersive fiber, a 2.3- and 20-km-long fiber with 17 ps/km–nm are used in the first and the second stage of the PDM, respectively. Although the lengths of the fibers used in this PDM do not increase exponentially along the stages, the

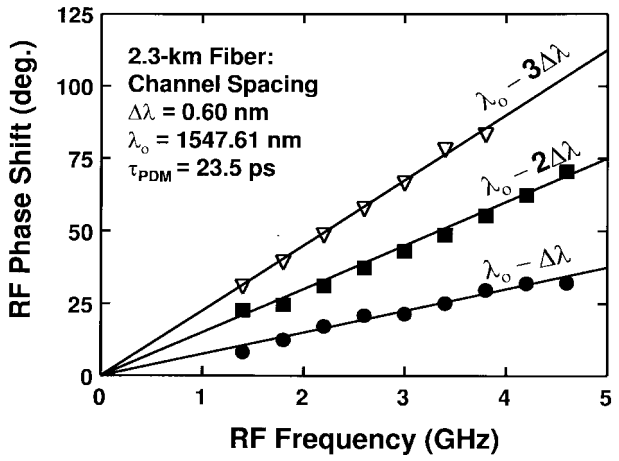

(a)

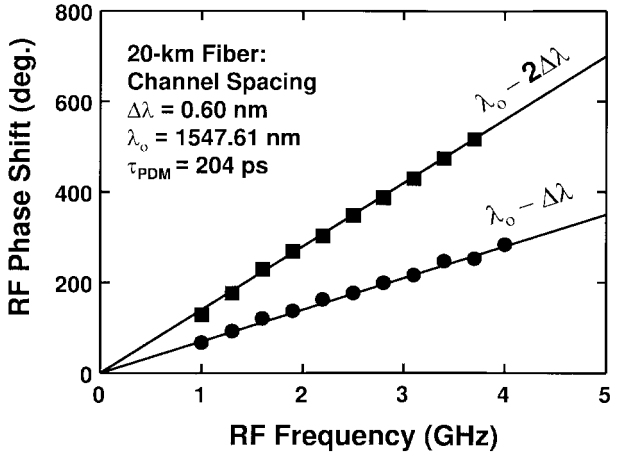

(b)

Fig. 6. Relative RF phase shift versus frequency generated by dispersive fiber for various optical wavelength relative to the reference optical channels at $\lambda_o = 1547.61$ nm. The length of the fibers are (a) 2.3 and (b) 20 km.

concept of dispersion-generated time delay among the optical channels can still be clearly demonstrated by this prototype. The RF signal is applied to all optical channels through an EO modulator with 5-GHz bandwidth. A tunable fiber Fabry–Perot filter with 0.15-nm bandwidth is placed after the PDM to select different optical channels for RF phase measurement. The selected channel is fed to a high-speed photodetector. The RF phase measurement is measured by an HP 8510 RF network analyzer. Fig. 6(a) and (b) shows the measured RF phase shifts induced by the 2.3- and 20-km fibers, respectively, as a function of RF frequency for various optical channels. All the measured phase shifts are relative to that at $\lambda = 1547.61$ nm. Very linear phase shift with frequency is observed for the entire bandwidth of the EO modulator. Using the 2.3- and 20-km fibers, relative time delays of 23.5 and 204 ps are obtained between adjacent optical channels. The length of the fiber can be reduced by using high dispersion.

The fiber-grating PDM is characterized by a similar setup with dispersive fibers replaced by fiber gratings. Each fiber has four Bragg gratings centered at 1546.85, 1547.47, 1548.09, and 1548.71 nm, which match the optical wavelengths of the CPM laser. The grating spacings in the first and the second

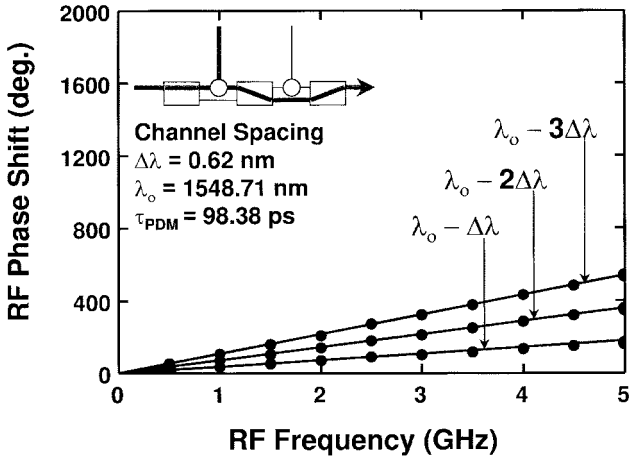

(a)

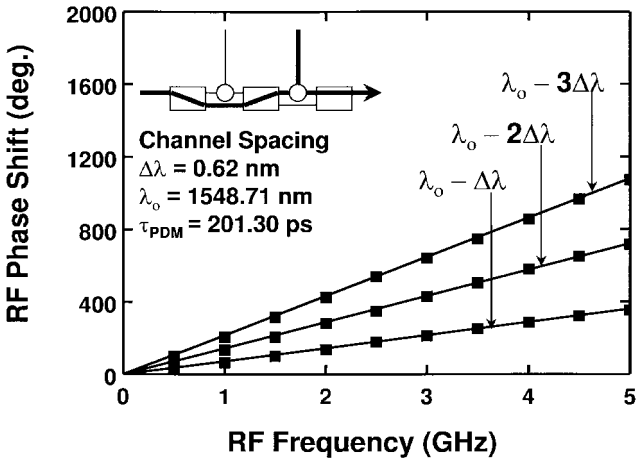

(b)

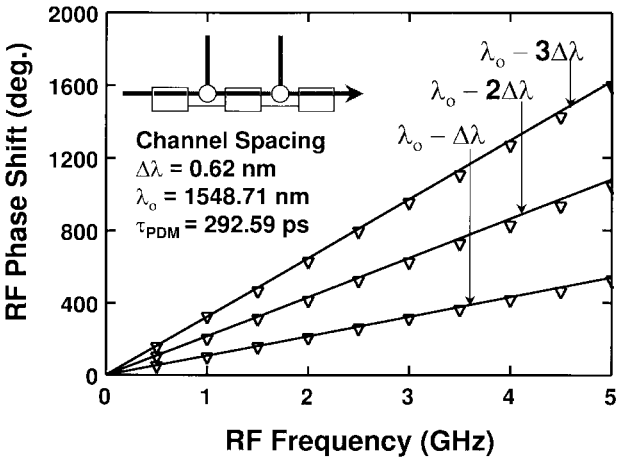

(c)

Fig. 7. Relative RF phase shift versus frequency generated by fiber grating PDM for various optical wavelength relative to the reference optical channels at $\lambda_o = 1548.71$ nm. The time delays measured in (a)–(c) are generated by the fiber grating in the first stage S_1, the second stage S_2, and both stages $S_1 + S_2$ of the PDM, respectively. The insets show the path of lightwave through the PDM.

stage of the PDM are 1 and 2 cm, respectively. All the gratings used in the setup have a reflectivity of 85% and a full width at half maximum (FWHM) bandwidth of 0.15 nm. Fig. 7(a)–(c) shows the measured RF phase shifts for

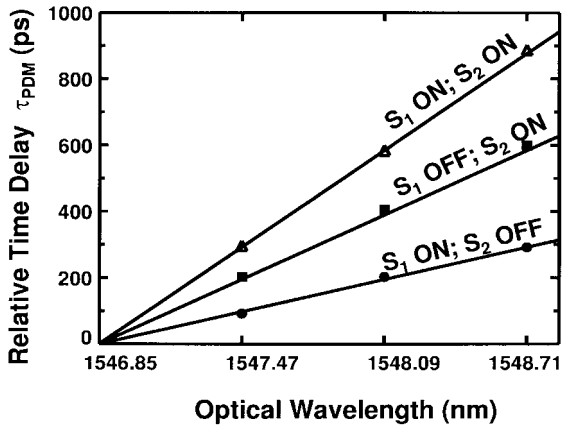

Fig. 8. Relative time delays measured among various optical channels by the gratings in the first stage S_1 and the second stage S_2 of the PDM.

various optical channels as a function of RF frequency. The phase shifts are measured relative to that at $\lambda = 1548.71$ nm. Linear phase shift spans over the entire bandwidth of the EO modulator is observed for all switching conditions of the PDM. The time delays among the optical channels corresponds to various switching states of the PDM is illustrated in Fig. 8. By routing the optical wavelengths through either/or both grating fibers, the measured time delays between adjacent wavelengths are 98.38, 201.30, and 292.59 ps, respectively, which agree well with the theoretical values of 97.33, 194.67, and 292 ps.

To measure the relative RF phase shifts among array elements of the 2-D MWOCPAA, a 4×2 MWOCPAA prototype with 2-b resolution in both planes is constructed. Fiber grating is used for beam steering in the elevation. The output of the PDM is split by a 1×2 optical coupler. An SODL with 2-b resolution is attached to one branch of the optical coupler. The lengths of the delay lines in the first and the second stages of the SODL are 1 and 2 cm, respectively. Fig. 9(a)–(c) shows the measured RF phase shifts for the second column of the array. These RF phase shifts are measured relative to the first element ($\lambda = 1546.85$ nm) in column one. In addition to the phase shifts among the elements in the same column, which are identical to Fig. 7(a), the column phase shift generated by the SODL is clearly indicated by the rotation of the data lines away from the x-axis in Fig. 9(a)–(c). The degree of rotation is proportional to the time delay between the two columns. The full set of time delays for column two is summarized in Fig. 10. The dotted line represents the wavelength-dependent relative time delay generated by the first fiber grating of the PDM only (same as that in Fig. 8). The solid lines are the time delays measured between the two columns by routing the lightwave through either delay lines, or both, of the SODL. The measured time delays between the two columns are 44.44, 98.33, and 150 ps, compared to the theoretical value 48.67, 97.33, and 146 ps, respectively.

V. Insertion Loss of PDM and SODL in MWOCPAA System

Since the PDM and the SODL comprise serially connected optical components, optical insertion loss is a potential concern for the RF performance of the system. The sources of optical loss include optical switches, reflection loss in fiber grating, and optical circulators. The total insertion loss of the PDM

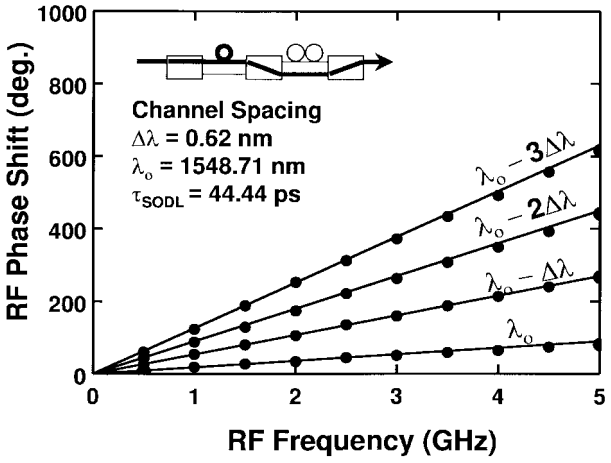

(a)

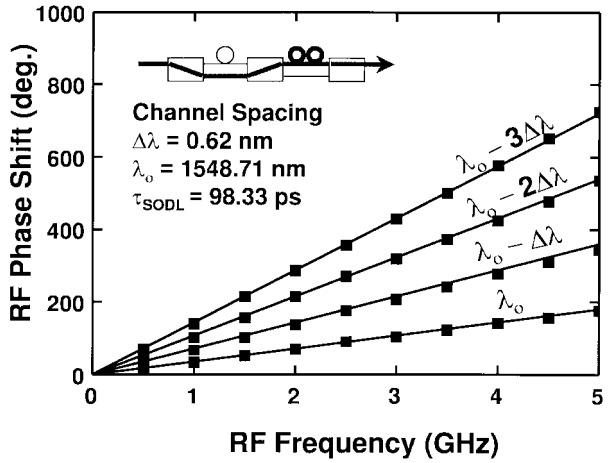

(b)

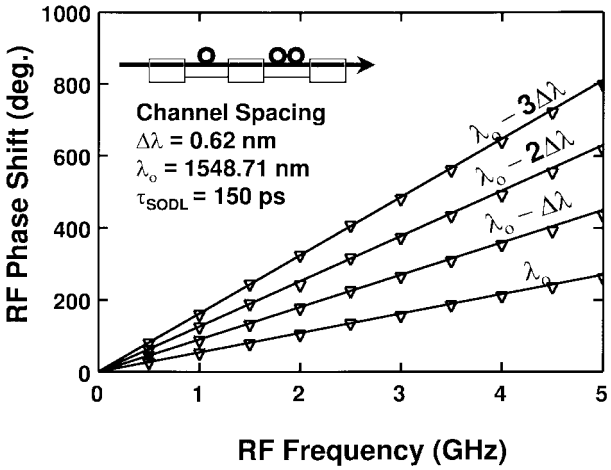

(c)

Fig. 9. Relative RF phase shifts measured for various optical channels in the second columns of the array, relative to the reference optical channels at $\lambda_o = 1548.71$ nm in the first column, generated by SODL in a 2-D MWOCPAA prototype. The RF phase shifts among different optical channels in the same column are controlled by the first stage in the fiber grating PDM. The operation of the SODL is indicated by the rotation of the lines away from x-axis. The insets show the path of lightwave through the SODL attached to the second column.

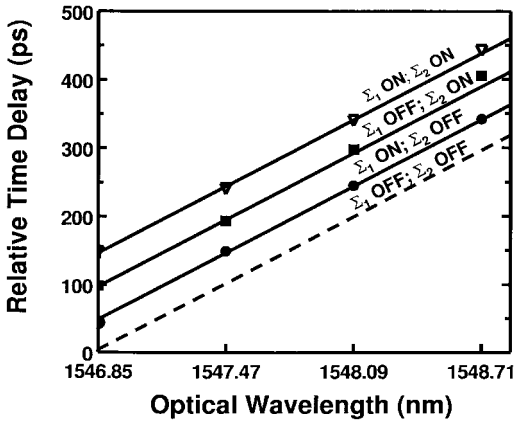

Fig. 10. Relative time delay measured between the two columns of the array generated by the first stage Σ_1 and the second stage Σ_2 of the SODL. The relative time delay among the optical wavelengths in the same column are maintained by the first fiber grating the PDM during these measurements. The dotted line indicates zero time delay between the two columns.

and the SODL are

$$\alpha_{\mathrm{PDM-DF}} = (n+1)\cdot\alpha_s \tag{7}$$

$$\alpha_{\mathrm{PDM-FG}} = (n+1)\cdot\alpha_s + n\cdot(2\cdot\alpha_c + \alpha_g) \tag{8}$$

$$\alpha_{\mathrm{SODL}} = (m+1)\cdot\alpha_s. \tag{9}$$

Here, $\alpha_{\mathrm{PDM-DF}}$, $\alpha_{\mathrm{PDM-G}}$, and α_{SODL} are the total insertion loss (in decibels) for the dispersive-fiber PDM, the fiber-grating PDM, and the SODL, respectively, α_s is the insertion loss of the optical switch, α_c is the single-pass insertion loss of the optical circulator, and α_g is the reflection loss of the grating. The fiber loss is assumed to be negligible. Typical values of the various loss are $\alpha_s = 1$ dB (for optomechanical switch), $\alpha_c = 1$ dB, and $\alpha_g = 0.5$ dB (assume a 90% grating reflectivity). A recently reported fiber-based acousto-optic (AO) switch [16] with similar α_s, but faster switching time can also be employed for faster beamforming (< 50 μs). As a result, $\alpha_{\mathrm{PDM-DF}}$, $\alpha_{\mathrm{PDM-G}}$ and α_{SODL} are equal to $(n+1)$, $(3.5\cdot n+1)$, and $(m+1)$ dB, respectively. It should be noted that the insertion loss of the fiber grating PDM is path dependent. The path-dependent insertion loss in a fiber grating PDM can be corrected by replacing the nondispersive fibers in the lower path at each PDM stage with: 1) optical attenuators to equalize the insertion loss or 2) fibers with gratings in reverse-wavelength order to construct a "push–pull" fiber-grating PDM.

The insertion loss of the PDM and the SODL can be compensated by optical amplifier. An erbium-doped fiber amplifier (EDFA) with high gain and low noise figure has been demonstrated [17]. It has been shown that the noise contributed by the EDFA is similar to that of a laser source with a higher effective relative intensity noise [18]. The effective relative intensity noise of the cascaded amplifiers, $\mathrm{RIN_{EFF}}$, can be related to the laser relative intensity noise, RIN_L, by [18]

$$\mathrm{RIN_{EFF}} = \mathrm{RIN_L} + \frac{2F_1E}{P_1} + \frac{2F_2E}{P_2} + \frac{2F_3E}{P_3} \tag{10}$$

where F_i and P_i are the noise figures and the input optical power of the optical amplifiers, respectively, and E is the photon energy. As an example, EDFA's with gains of 15 and 20 dB are placed at the input and the output of the 10-b fiber-grating PDM, respectively, for loss compensation in a 32-element 1-D MWOCPAA. To achieve better $\mathrm{RIN_{EFF}}$, an additional EDFA with a gain of 15 dB is inserted within the PDM (after the 5th PDM stage). All EDFA's are assumed to have noise figures of 4 dB ($F_i = 2.5$). The gains of the EDFA's are selected so that no optical output power exceeds the saturation power of 20 dBm. The initial input optical power is $P_1 = -10$ dBm/wavelength. For a laser relative intensity noise of $\mathrm{RIN}_L = -165$ dB/Hz, the $\mathrm{RIN_{EFF}}$ calculated from (10) is -133.6 dB/Hz. Including a 4-dB insertion loss of the WDM demultiplexer, an optical power of 0 dBm/wavelength at the antenna element is obtained. The excessive noise figure introduced by the EDFA's is 10.8 dB (assume a 4% optical modulation index). Similar excessive noise figure can be obtained in 2-D MWOCPAA.

The insertion loss of the fiber-grating PDM can also be reduced by combining dispersive fiber and fiber grating in the PDM. For example, the insertion loss of a 10-b PDM that employs dispersive fibers in the first five stages and fiber gratings in the last five stage is reduced by 12.5 dB compared to a 10-b fiber-grating PDM. Dispersive fibers could reduce the bandwidth of the system. By keeping the dispersive fibers in the first few stages (shorter relative time delays), reasonable system bandwidth can be maintained. The length of standard single-mode fiber in this example is on the order of 400 m, which has an instantaneous bandwidth of 60 GHz at 1-dB penalty on RF carrier [12]. A more attractive approach is to employ PDM without optical circulators since they contribute 2-dB loss per stage. For example, cascaded contradirectional grating-assisted couplers [19] can be used to replace the fiber grating. They are transmission devices and do not need optical circulator, wavelengths are reflected at different positions along the input waveguide and coupled to output waveguide. Our calculation shows that a reflectivity of $>90\%$ for each optical wavelength can be achieved in this type of device.

VI. Array Size and Optical-Wavelength Demultiplexing

With strict one-to-one correspondence between optical wavelengths and array elements, the array size could be limited by the number of optical wavelength channels in the WDM source and demultiplexer. Currently, monolithic multiwavelength DFB laser arrays with 40 optical wavelengths has been reported [11], and up to 50 optical wavelengths have been used in advanced WDM networks [20]. The array size can further be multiplied by using each optical wavelength to feed microwave subarray or by partition the array into subarrays, each equipped with its own multiwavelength source and PDM.

The WDM couplers with low crosstalk between adjacent channels should be employed for MWOCPAA since optical crosstalk directly impacts the isolation between antenna elements. The optical crosstalk can be reduced by increasing the channel spacing. However, this might limit the total number of

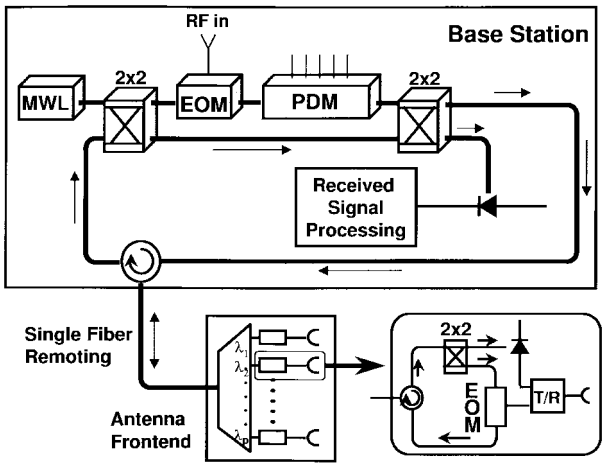

Fig. 11. Schematic diagram of MWOCPAA common T/R module.

wavelengths available. The tradeoff between crosstalk and the number of channels needs to be optimized. Subarrays might need to be used to satisfy both the requirement of channel isolation and array size. Integrated arrayed-waveguide grating demultiplexer designed for WDM telecommunication with 32 channels and <28 $\mathrm{dB_{optical}}$ interchannel crosstalk has been reported [21] and is a potential candidate for this application. This yields an isolation between adjacent array elements of < 56 $\mathrm{dB_{electrical}}$ between adjacent antenna elements. Similar device with larger channel capacity (128) will favor larger array—however, at the expense of higher crosstalk [22]. It should be mentioned that the continual rapid advances in WDM components driven by the telecommunication industry will further improve the performance of the MWOCPAA.

VII. MWOCPAA T/R Module in 1-D System

In most antenna applications, both transmit and receive operations are required. Moreover, a common T/R module is preferable for a low-cost integrated system. Fig. 11 shows the schematic diagram of the T/R module for the 1-D MWOCPAA. The T/R module is similar to the transmitter described in Section II except that additional optical switches and circulators are incorporated to switch between the transmit and receive modes. When the switches are in the bar state, the T/R module operates in transmit mode. When the switches are in cross state, the module operates in the receive mode. The optical wavelengths are sent to the antennas without passing through the PDM or the EO modulator in the base station. After being modulated by the received RF signals, the optical wavelength are combined through the WDM coupler and sent to the PDM for TTD processing. The processed multiwavelength signals are then combined in a photodetector. The total photocurrent is proportional to the sum of the receiving RF signal. Compared to other proposed receiver schemes [3], the MWOCPAA T/R module can achieve wide instantaneous bandwidth in the receive mode because no RF mixer are required in the system. Moreover, by employing different optical wavelengths for each antenna element, optical combining of the received RF signals in the optical domain can be achieved without suffering from optical coherent effect.

VIII. Conclusion

In conclusion, we have proposed and demonstrated a hardware-compressive MWOCPPA in both 1-D and 2-D architecture. In general, a $p \times q$ MWOCPAA with n-b $\times$ m-b scanning resolution only requires one multiwavelength laser source with p optical wavelength channels, one n-b PDM, one $1 \times q$ optical coupler, $(q-1)$ m-b SODL's, and q WDM demultiplexers. The feasibility of this multiwavelength scheme using PDM and SODL is experimentally demonstrated by a 4×2 MWOCPAA prototype with 2-b resolution in both scan directions. The TTD processing is performed in parallel on all the optical channels and, therefore, the amount of hardware required for this scheme is significantly reduced. Extension of this multiwavelength scheme to receive mode and T/R module is also described. The MWOCPAA receive mode allows TTD processing with large instantaneous bandwidth. All these remarkable features make the MWOCPAA system attractive for future high-performance radar and communication systems.

Acknowledgment

The authors wish to thank Prof. H. R. Fetterman of UCLA, Dr. J. C. Brock of TRW, Redondo Beach, CA, Dr. C. E. Zah of Bellcore, Red Bank, NJ, and Dr. B. M. Hendrickson of DARPA/ROME, for fruitful discussion. They also thank Dr. N. Kwong of Ortel Corporation, Alhambra, CA, and Dr. J. Simpson of Lucent Technologies, Bell Laboratories, Murray Hill, NJ, for providing the fibers used in this experiment, and M. Ichimura of Sumitomo Company, Los Angeles, CA, who kindly provided the modulator.

References

[1] W. Ng, A. A. Walston, G. Tangonan, J. J. Lee, and I. L. Newberg, "The first demonstration of an optically steered microwave phased array antenna using true-time-delay," *J. Lightwave Technol.*, vol. 9, pp. 1124–1131, Sept. 1991.

[2] R. Soref, "Optical dispersion technique for time-delay beam steering," *Appl. Opt.*, vol. 31, pp. 7395–7397, Dec. 1992.

[3] M. Y. Frankel, R. D. Esman, and M. G. Parent, "Array transmitter/receiver controlled by a true time-delay fiber-optic beamformer," *IEEE Photon. Technol. Lett.*, vol. 7, pp. 1216–1218, Oct. 1995.

[4] A. Goutzoulis and K. Davies, "Development and field demonstration of a hardware-compressive fiber-optic true-time delay steering system for phased-array antennas," *Opt. Eng.*, vol. 3, pp. 8173–8185, Dec. 1994.

[5] P. M. Freitag and S. R. Forrest "A coherent optically controlled phased array antenna system," *IEEE Microwave Guided Wave Lett.*, vol. 3, pp. 293–295, Sept. 1993.

[6] J. Lembo, T. Holcomb, M. Wickham, P. Wisseman, and J. C. Brock, "Low-loss fiber optic time-delay element for phased-array antennas," in *Proc. SPIE-Int. Soc. Opt. Eng.*, vol. 2155, pp. 13–23, 1994.

[7] Y. Chang, B. Tsap, H. R. Fetterman, D. A. Cohen, A. F. Levi, and I. L. Newberg, "Optically controlled serially fed phased-array transmitter," *IEEE Microwave Guided Wave Lett.*, vol. 7, pp. 69–71, Mar. 1997.

[8] D. T. K. Tong and M. C. Wu, "A novel multiwavelength optically controlled phased array antenna with a programmable dispersion matrix," *IEEE Photon. Technol. Lett.*, vol. 8, pp. 812–814, June 1996.

[9] ——, "Programmable dispersion matrix using Bragg fiber grating for optically controlled phased array antennas," *Electron. Lett.*, vol. 32, no. 17, pp. 1532–1533, Aug. 1996.

[10] C. E. Zah, F. J. Favire, B. Pathak, R. Bhat, C. Caneau, P. S. Lin, A. S. Gozdz, N. C. Andreadakis, M. A. Koza, and T. P. Lee, "Monolithic integration of multiwavelength compressive-strained multiquantum-well distributed-feedback laser array with star coupler and optical amplifier," *Electron. Lett.*, vol. 28, pp. 2361–2362, Dec. 1992.

[11] K. Kudo, H. Yamazaki, T. Sasaki, and M. Yamaguchi, "Over 75-nm-wide wavelength range detuning-adjusted DFB-LD's of different

wavelengths fabricated on a wafer," presented at the *OFC'97*, Dallas, TX, Feb. 1997.
[12] U. Gliese, S. Nørskov, and T. N. Nielsen, "Chromatic dispersion in fiber-optic microwave and millimeter-wave links," *IEEE Trans. Microwave Theory Tech.*, vol. 44, pp. 1716–1724, Oct. 1996.
[13] A. P. Goutzoulis, D. K. Davies, and J. M. Zomp, "Prototype binary fiber optic delay line," *Appl. Opt.*, vol. 28, pp. 1193–1202, Nov. 1989.
[14] Y. K. Chen and M. C. Wu, "Monolithic colliding-pulse mode-locked quantum-well lasers," *IEEE J. Quantum Electron.*, vol. 28, pp. 2176–2185, Oct. 1992.
[15] P. T. Ho, "Phase and amplitude fluctuations in a mode-locked laser," *IEEE J. Quantum Electron.*, vol. QE-21, pp. 1806–1813, Nov. 1985.
[16] D. O. Culverhouse, R. I. Laming, S. G. Farwell, T. A. Birks, and M. N. Zervas, "All fiber 2 × 2 polarization insensitive switch," *IEEE Photon. Technol. Lett.*, vol. 9, pp. 455–457, Apr. 1997.
[17] R. I. Laming, M. N. Zervas, and D. N. Payne, "Erbium-doped fiber amplifier with 54 dB gain and 3.1 dB noise figure," *IEEE Photon. Technol. Lett.*, vol. 4, pp. 1345–1347, Dec. 1992.
[18] W. I. Way, C. E. Zah, and T. P. Lee, "Application of travelling-wave laser amplifiers in subcarrier multiplexed lightwave systems," *IEEE Trans. Microwave Theory Tech.*, vol. 38, pp. 534–545, May 1990.
[19] P. Yeh and H. F. Taylor, "Contradirectional frequency-selective couplers for guided-wave optics," *Appl. Opt.*, vol. 19, pp. 2848–2855, Aug. 1980.
[20] A. H. Gnauck, A. R. Chraplyvy, R. W. Tkach, J. L. Zyskind, J. W. Sulhoff, A. J. Lucero, Y. Sun, R. M. Jopson, F. Forghieri, R. M. Derosier, C. Wolf, and A. R. McCormick, "One Terabit/s transmission experiment," presented at the *OFC'96*, San Jose, CA, Feb. 1996.
[21] Y. Tachikawa, Y. Inoue, M. Ishii, and T. Nozawa, "Arrayed-waveguide grating multiplexer with loop-back optical paths and its applications," *J. Lightwave Technol.*, vol. 14, pp. 977–984, June 1996.
[22] K. Okamoto, K. Syuto, H. Takahashi, and Y. Ohmori, "Fabrication of 128-channel arrayed-waveguide grating multiplexer with 25 GHz channel spacing," *Electron. Lett.*, vol. 32, pp. 1474–1476, Aug. 1996.

Dennis T. K. Tong received the B.S. degree from the University of Maryland at College Park, in 1993, the M.S. degree from the University of California at Los Angeles (UCLA), in 1995, both in electrical engineering, and is currently working toward the Ph.D. degree.

His research interests include OCPPA's, optoelectronic transmission of millimeter-wave, and WDM laser source.

Ming C. Wu (S'82–M'83) received the M.S. and Ph.D. degrees in electrical engineering from the University of California at Berkeley, in 1985 and 1988, respectively.

From 1988 to 1992, he was a Member of the technical staff at AT&T Bell Laboratories, Murray Hill, NJ, where he conducted research in high-speed semiconductor lasers and optoelectronics. In 1993, he joined the faculty of the Electrical Engineering Department, University of California at Los Angeles (UCLA), as an Associate Professor. His current research interests include micromachined optical systems, optical MEMS, free-space integrated optics, ultrafast integrated optoelectronics, microwave and millimeter-wave photonics, high-power photodetectors, semiconductor lasers, and optical interconnect. He has published over 80 papers in research journals, 110 papers in refereed conferences, contributed one book chapter, and holds eight U.S. patents.

Dr. Wu is a member of the American Physical Society, Optical Society of America, URSI, and Eta Kappa Nu. He has served as general co-chair for the IEEE Lasers and Electro-Optics Society (LEOS) Summer Topical Meeting on Optical MEMS in 1996 and RF Optoelectronics in 1995. He also served as program committee chair for the 1997 IEEE LEOS Topical Meeting on Optical MEMS, and served on the Program Committee of CLEO in 1996 and 1997, IEDM in 1996, and Photonic West in 1997. He was the recipient of the Packard Foundation Fellow in 1992, and the Meritorious Conference Paper Award of the 1994 GOMAC.